Migration-velocity analysis using image-space generalized wavefields

Claudio Guerra* (Petrobras), Biondo Biondi (Stanford University)

Abstract

We show 3D real data results of migration-velocity analysis by wavefield extrapolation using data synthesized by the prestack exploding-reflector model. The prestack exploding-reflector model generalizes the exploding-reflector model in a sense that migration of prestack exploding-reflector model data generates a prestack image. Phase-encoding the modeling experiments drastically reduces data size, allowing fast migration-velocity analysis. Also, since the modeling can be limited to a region with inaccurate velocity, a target-oriented strategy can be applied in migration-velocity analysis. The initial conditions for the modeling are reflectors interpreted in a prestack image computed by wavefield-extrapolation methods. Hence, a horizon-based strategy is naturally incorporated into migration-velocity analysis by wavefield-extrapolation.

Introduction

In areas of complex geology, migration by wavefield extrapolation has been widely used because it properly handles complex distortions of the wavefields. However, even though in those areas migration-velocity analysis (MVA) by wavefield extrapolation (Sava and Biondi, 2004; Shen and Symes, 2008) promises to produce more reliable results, it has been rarely used (Fei et al., 2009) due to the high computational cost and lack of flexibility to parameterize the model space. In consequence, ray-based methods are the industry standards. Hence, to turn MVA by wavefield extrapolation of practical use, we face the challenge of decreasing its cost and increasing its flexibility while maintaining its robustness.

A typical way of decreasing the cost of wavefield extrapolation is to reduce the amount of input data by linearly combining the wavefields using plane-wave phase-encoding and random phase-encoding, for instance. This linear combination expands the concept of point sources to generalized sources. Commonly, generalized sources are synthesized in the data space. However, when linearly combined wavefields are initiated in the image space, image-space generalized wavefields are generated. Combination of wavefields initiated in the image space is exploited by the prestack-exploding reflector model (PERM) (Biondi, 2006) to significantly reduce the data size while keeping the migrated image crosstalk-free. This is achieved by selecting from a prestack image computed by wavefield-extrapolation methods subsurface-offset common-image gathers (SODCIGs) separated by a decorrelation distance such that the wavefields from different SODCIGs in the same modeling experiment do not correlate during migration. Guerra et al. (2009) show that further reduction can be achieved by randomly phase-encoding the modeling experiments, which generates the image-space phase-encoded wavefields (ISPEWs), significantly decreasing the cost of MVA iterations. Since PERM wavefields and ISPEWs are generalized wavefields initiated in the image space, we call them image-space generalized wavefields.

In 3D, reduction of the data size can be considerable if the initial image used to model PERM wavefields has only inline subsurface offsets, as in the common-azimuth approximation. In this case, Guerra (2010) shows that data size can be two orders of magnitude smaller than 3D-plane wave data.

Another interesting feature of PERM is that, because the wavefields are upward propagated, data can be collected at any depth level. In MVA, PERM wavefields can be propagated only in the region with velocity inaccuracies, such that velocity update can be performed in a target-oriented way, which contributes to an additional cost reduction of migration velocity analysis.

We present the modeling of PERM wavefields and ISPEWs, discuss the use of these wavefields in MVA by wavefield extrapolation, and illustrate it using a 3D dataset from the North Sea.

The prestack exploding-reflector model

The fundamental idea of PERM is to synthesize areal shots whose migration describes the correct kinematics of a reflector in an isolated SODCIG computed with wavefield-extrapolation methods. This is achieved by downward and upward extrapolating wavefields starting from the prestack image at the vicinity of the SODCIG. The modeling of downward (D) and upward (U) PERM wavefields can be carried out by any wavefield-continuation scheme. Here, we use the following one-way wave equations:

$$\begin{cases} \left(\dfrac{\partial}{\partial z} - i\sqrt{\omega^2 s_0^2 - |\mathbf{k}|^2} \right) D(\mathbf{x}, \omega; \mathbf{x_m}) = I_D(\mathbf{x}, \mathbf{h}) \\ D(x, y, z = z_{\max}, \omega; \mathbf{x_m}) = 0 \end{cases}, \quad (1)$$

and

$$\begin{cases} \left(\dfrac{\partial}{\partial z} + i\sqrt{\omega^2 s_0^2 - |\mathbf{k}|^2} \right) U(\mathbf{x}, \omega; \mathbf{x_m}) = I_U(\mathbf{x}, \mathbf{h}) \\ U(x, y, z = z_{\max}, \omega; \mathbf{x_m}) = 0 \end{cases}, \quad (2)$$

where ω is frequency, $\mathbf{h}$ is the subsurface offset, s_0 is the background slowness also used in the migration of the

initial image, and I_D and I_U are prestack images used as the initial conditions for the modeling of downward and upward wavefields, respectively, and are computed by rotating the original image according to the apparent geological dip. This rotation is necessary to correct for the image-point dispersal (Biondi and Symes, 2004) when an inaccurate migration velocity is used in the presence of dip. The rotation of SODCIGs is extensively discussed in Guerra (2010). Using SODCIGs separately in the modeling can originate PERM data even bigger than the original data. By combining the modeling experiments, respecting a decorrelation distance between SODCIGs simultaneously injected, drastically decreases the imaging cost. This decorrelation distance is necessary to avoid crosstalk during imaging and must be at least twice the subsurface-offset range.

Image-space phase-encoded wavefields

The image-space phase-encoded wavefields (ISPEWs) are computed using PERM along with phase-encoding techniques to further improve data reduction achieved with PERM. The phase-encoding is performed during the modeling, in which reflectors are encoded using a particular coding sequence. This allows injection of multiple reflectors and SODCIGs more closely spaced than the decorrelation distance, while diminishing the prejudicial effect of crosstalk during imaging. To be properly encoded, reflectors must be identified in the prestack volume $I(\mathbf{x},\mathbf{h})$. The interpretation and selection of key reflectors naturally incorporate a horizon-based strategy into MVA by wavefield extrapolation. The SODCIGs are encoded according to:

$$\hat{I}(\hat{\mathbf{x}},\mathbf{h},\mathbf{q};\omega)=\sum_m \sum_j \delta(\hat{\mathbf{x}}-m\Delta x)e^{i\gamma(\hat{\mathbf{x}},j,\mathbf{q},\omega)} \times W_j(\hat{\mathbf{x}},\mathbf{h})I(\hat{\mathbf{x}},\mathbf{h}), \quad (3)$$

where the delta function denotes the selection of the SODCIGs separated by the distance Δx, W selects the reflector j, $\mathbf{q}$ is the realization index, and γ can be any pseudo-random sequence. ISPEWs can be modeled within a region of velocity inaccuracy and collected at its top. This allows MVA by wavefield extrapolation to be easily solved in a target-oriented manner.

MVA using ISPEW

The theory of MVA by wavefield extrapolation in the image-space generalized sources domain was described by Guerra et al. (2009). In this domain, PERM wavefields and ISPEW are the carriers of information. They allow fast velocity updates due to the small data size and to their inherent capability for being used in a target-oriented manner. These wavefields enable us to incorporate well-established strategies used in ray-based MVA, such as horizon-based tomography and possibly grid-based tomography, into MVA by wavefield extrapolation. This new feature gives more flexibility to MVA by wavefield extrapolation and can improve convergence to an optimal velocity. MVA by wavefield extrapolation can be performed by wave-equation migration velocity analysis (WEMVA) (Sava and Biondi, 2004) and differential-semblance velocity analysis (DSVA) (Shen and Symes, 2008). Here, we use DSVA, in which a nonlinear conjugate-gradient method is drives to a minimum the objective function

$$J(s)=\frac{1}{2}\left\|\Delta\hat{I}\right\|_2^2=\frac{1}{2}\left\|\mathbf{H}\hat{I}\right\|_2^2 \quad (4)$$

where $\Delta\hat{I}$ is the perturbed image computed by applying the DSO operator $\mathbf{H}$ on the background image $\hat{I}$ computed with the current velocity. The DSO operator weights an image with the absolute value of the subsurface offset. In the reflection-angle domain, it corresponds to compute the derivative along the reflection-angle dimension.

To update the current velocity model, we need to compute the slowness perturbation derived from the gradient of the objective function in equation 4 with respect to the slowness. Figure 1 synthesizes the computation of the slowness perturbation using 35 ISPEWs synthesized from 12 reflectors for a portion of the Marmousi model. The yellow triangles show the approximated position of the SODCIGs on the right. The scattered wavefields $\hat{D}_{sc}$ and $\hat{U}_{sc}$ are computed by applying the scattering operator $\mathbf{B}$ (Huang et al., 1999) on the background wavefields $\hat{D}_0$ and $\hat{U}_0$ and extrapolating them to the next depth level with the operator $\mathbf{T}$. The perturbed wavefields $\Delta\hat{D}$ and $\Delta\hat{U}$ are computed by convolving the background wavefields with the perturbed image. Finally, cross-correlating scattered and perturbed wavefields generates the slowness perturbation. The bar represents complex conjugate. Velocity is to be updated only below the black line, where the initial velocity is smoother and 10% slower on average than the original velocity. To mitigate illumination imperfections and to provide smooth updates, the gradient is B-spline smoothed.

3D-Field data example

Using 3D-ISPEWs in IMVA by wavefield-extrapolation is illustrated with a 3D seismic data from the North Sea (50 km^2). The challenges of this dataset for defining the velocity model are a salt body with irregular shape and intense faulting, amplitude variations caused by irregular acquisition, short offsets (3600 m maximum), and limited azimuths. The 3D dataset was submitted to azimuth-moveout (AMO), and common-azimuth migrated images are used as the initial conditions for the modeling of only 30 3D-ISPEWs. SODCIGs are continuously injected in the cross-line direction to model 3D-ISPEWs, since no cross-line offset is computed in common-azimuth migration (CAM). The initial velocity model (Figure 2a) results from refining the sediment velocity above the upper chalk using 3D residual-MVA. Therefore, velocity for the shallow sediments is considered to be sufficiently accurate and does not need to be optimized. Also, below the top of the upper chalk, the initial velocity model results from smoothing and 10% scaling down a velocity model defined using a ray-based method. In the MVA strategy, for the upper chalk layer, only one reflector (base of

chalk) is used in the modelling of 30 3D-ISPEWs, whereas seven reflectors were injected to model 30 3D-ISPEWs for the sub-salt and sub-chalk sediments. A horizon-based strategy, along with salt-flooding, was used in the velocity inversion, yielding consistent velocity updates, fast convergence, and a geologically plausible velocity model (Figure 2b) obtained after seven iterations of nonlinear conjugate gradients using the MVA strategy previously described and depicted in Figure 3.

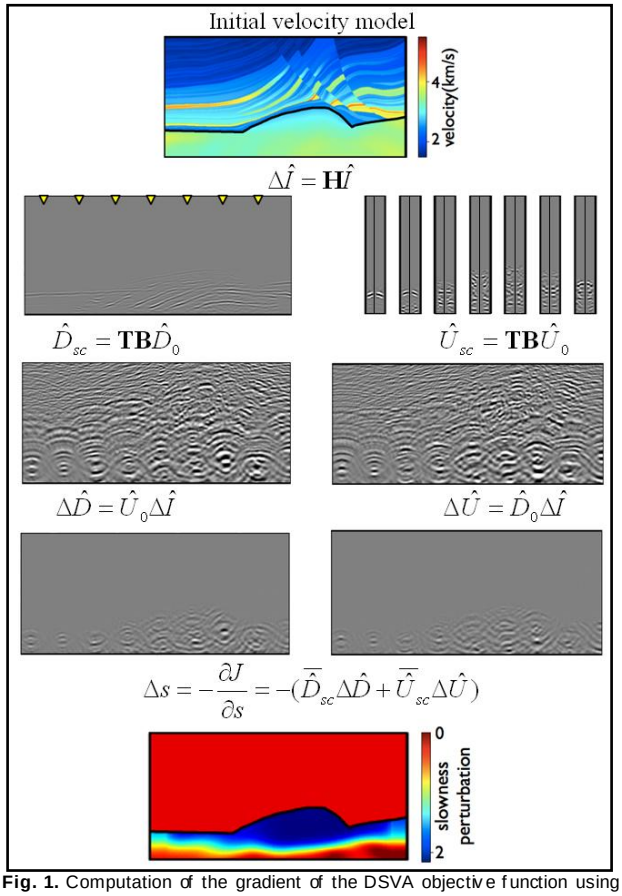

Fig. 1. Computation of the gradient of the DSVA objective function using ISPEW.

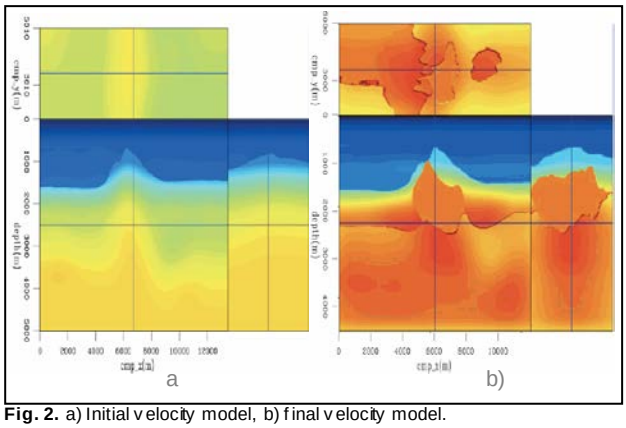

Fig. 2. a) Initial velocity model, b) final velocity model.

CAM images computed with the velocity models of Figure 2 and with the velocity model defined with a ray-based method are sown in Figure 4. It is clear the better focusing of the reflectors, imaging of faults, and definition of the salt body contours of the image computed with the final velocity model (Figure 4c) compared to that using the initial velocity model (Figure 4a) and the original velocity model (Figures 4b). Image quality and flatness of reflectors in the angle gathers confirms the greater accuracy of the final velocity model (Figure 5) over the original velocity model defined using ray-tracing (Figure 6). In both figures, on the top is the zero subsurface-offset section and at the bottom are the reflection-angle gathers. When migrating with the final velocity model reflectors are flatter in the angle gathers than when migrating with the original velocity model, especially below the salt and on the right flank as highlighted by the ovals.

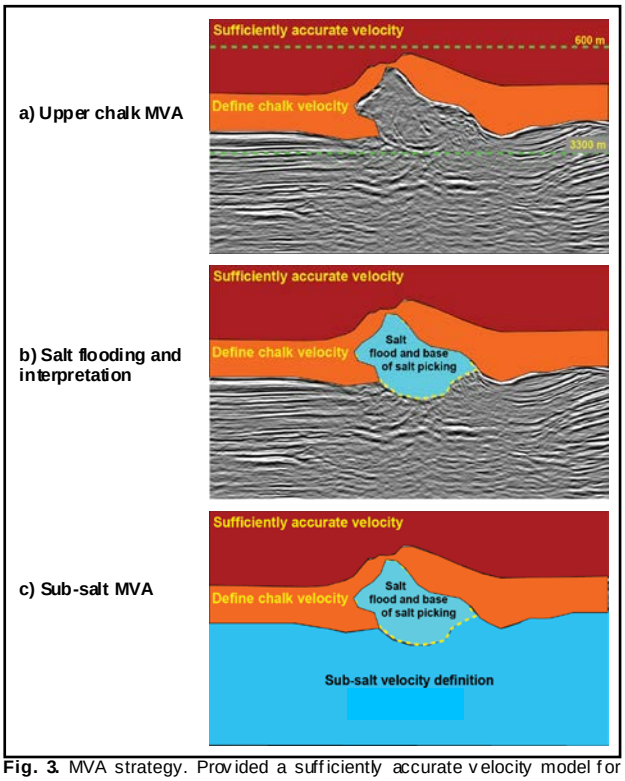

Fig. 3. MVA strategy. Provided a sufficiently accurate velocity model for the shallow sediments, in a) the upper chalk velocity model is defined using 30 3D-IDPEWs synthesized from the base of chalk, in b) we define the salt geometry, and in c) seven reflectors are injected to model 30 3D-IDPEWs used to update velocity below the salt.

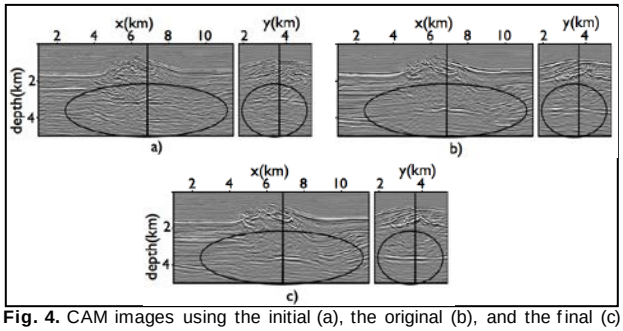

Fig. 4. CAM images using the initial (a), the original (b), and the final (c) velocity.

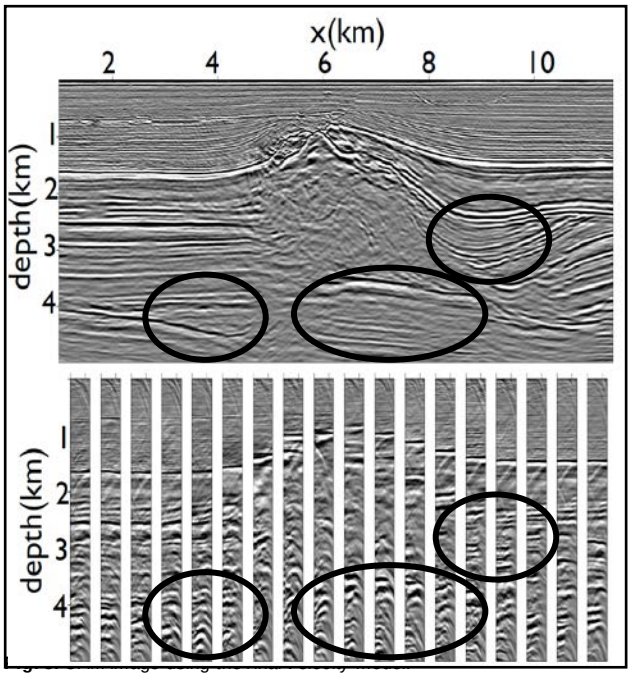

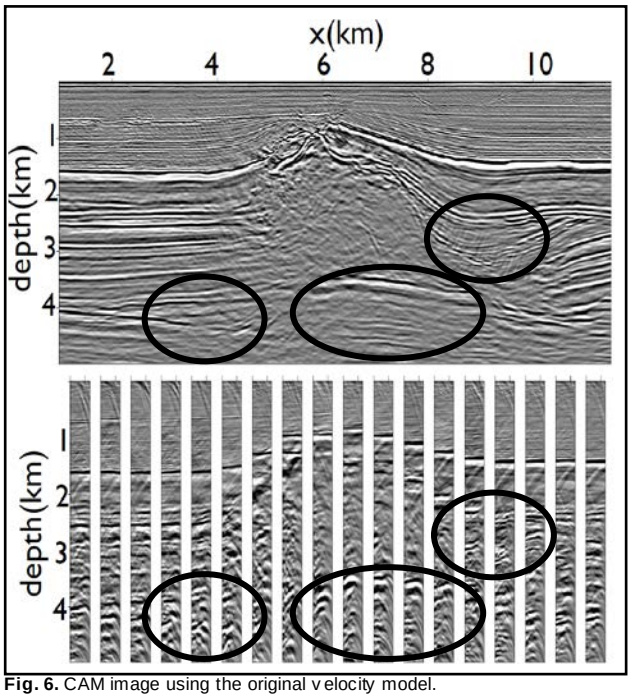

Fig. 6. CAM image using the original velocity model.

Conclusions

We introduced the image-space generalized wavefields, which are synthesized with the prestack exploding-reflector model. When phase encoded, these wavefields originate the image-space phase-encoded wavefields. Using 3D ISPEW has proven to greatly accelerate 3D-MVA by wavefield extrapolation, thanks to the small number of wavefields needed to satisfactorily describe the kinematics of the prestack image and the fact that they can be computed in a target-oriented manner.

With the great availability of computational resources, using 3D ISPEW can turn MVA by wavefield extrapolation an interactive process, which can yield more accurate and geologically reasonable solutions. In a 3D example from the North Sea, with only 30 ISPEW we were able to determine an accurate migration-velocity model, using different strategies like layer stripping and based on horizons.

Besides the computational gain, 3D ISPEWs were able to provide reliable velocity updates. Using the final velocity model produces a CAM image with quality superior to that obtained with the initial velocity model, as expected. Moreover, the image computed with the final velocity model is more accurate than that computed with the original velocity model, defined with a ray-tracing method, with better focusing and continuity of the sub-salt reflectors. The computational efficiency, flexibility, and velocity accuracy obtained with data computed by the prestack exploding-reflector model enables the use of MVA by wavefield extrapolation as a routine procedure to define migration velocity in areas of complex geology.

Acknowledgements

The authors would like to thank the sponsors of the Stanford Exploration Project for the financial support and TotalFinaElf for providing the field data. Claudio Guerra is indebted with Petrobras for all the support during his PhD.

References

Biondi, B., 2006, Prestack exploding-reflectors modeling for migration velocity analysis. SEG Technical Program Expanded Abstracts, 25, 3056.

Biondi, B. and W. W. Symes, 2004, Angle-domain common-image gathers for migration-velocity analysis by wavefield-continuation imaging. Geophysics, 69, 1283–1298.

Fei, W., P. Williamson, and A. Khoury, 2009, 3-D common-azimuth wave-equation migration velocity analysis. SEG Technical Program Expanded Abstracts, 28, 2283–2287.

Guerra, C., Tang, Y. and Biondi, B., 2009, Wave-equation tomography using image-space phase-encoded data. SEG Technical Program Expanded Abstracts, 28, 3964.

Guerra, C., 2010, Migration-velocity analysis using image-space generalized wavefields. *PhD thesis, Stanford University*.

Huang, L., Fehler, M., and Wu, R., 1999, Extended local Born Fourier migration method. Geophysics, 64, 1524.

Sava, P. and Biondi, B. ,2004, Wave-equation migration velocity analysis-I: Theory. Geophysical Prospecting, 52, 593.

Shen, P. and Symes, W., 2008, Automatic velocity analysis via shot-profile migration. Geophysics, 73, VE49.